

1           **Exploring Chemistry in Micro-Compartments using Guided Droplet**  
2 **Collisions in a Branched Quadrupole Trap Coupled to a Single Droplet, Paper**  
3           **Spray Mass Spectrometer**

4 Michael I. Jacobs,<sup>1,2</sup> James F. Davies,<sup>2</sup> Lance Lee,<sup>2,†</sup> Ryan D. Davis,<sup>2</sup> Frances Houle,<sup>2</sup> Kevin R.  
5 Wilson<sup>2,\*</sup>

6  
7 <sup>1</sup>Department of Chemistry, University of California, Berkeley, CA 94720, United States

8 <sup>2</sup>Chemical Sciences Division, Lawrence Berkeley National Laboratory, Berkeley, CA 94720,  
9 United States

10 <sup>†</sup>Now at Stanford Linear Accelerator Center, Menlo Park, CA 94025

11  
12 \* Correspondence to: [krwilson@lbl.gov](mailto:krwilson@lbl.gov), (510) 495-2474

13  
14 **Abstract:**

15 Recent studies suggest that reactions in aqueous micro-compartments can occur at significantly  
16 different rates than those in the bulk. Most studies have used electrospray to generate a  
17 polydisperse source of highly charged microdroplets, leading to multiple confounding factors  
18 potentially influencing reaction rates (e.g., evaporation, charge, size). Thus, the underlying  
19 mechanism for the observed enhancement remains unclear. We present a new type of  
20 electrodynamic balance—the branched quadrupole trap (BQT)—which can be used to study  
21 reactions in microdroplets in a controlled environment. The BQT allows for condensed phase  
22 chemical reactions to be initiated by colliding droplets with different reactants and levitating the  
23 merged droplet indefinitely. The performance of the BQT is characterized in several ways. Sub-  
24 millisecond mixing times as fast as ~400  $\mu\text{s}$  are measured for low velocity (~0.1 m/s) collisions of  
25 droplets with <40  $\mu\text{m}$  diameters. The reaction of ortho-phthalaldehyde (OPA) with alanine in the  
26 presence of dithiothreitol is measured using both fluorescence spectroscopy and single droplet  
27 paper spray (PS) mass spectrometry. The bimolecular rate constant for reaction of alanine with  
28 OPA is found to be  $84 \pm 10$  and  $67 \pm 6 \text{ M}^{-1} \text{ s}^{-1}$  in a 30  $\mu\text{m}$  radius droplet and bulk solution,  
29 respectively, which demonstrates that bimolecular reaction rate coefficients can be quantified  
30 using merged microdroplets and that merged droplets can be used to study rate enhancements due  
31 to compartmentalization. Products of the reaction of OPA with alanine are detected in single  
32 droplets using paper spray mass spectrometry. We demonstrate single droplets with <100 pg  
33 analyte can easily be studied using single droplet mass spectrometry.

## 34 I. Introduction

35 Chemical reactions in micron-sized compartments are ubiquitous in nature, occurring in  
36 cells, mineral pores, and atmospheric aerosols. Several recent studies suggest that reactions in  
37 confined spaces occur at enhanced rates that can be several orders of magnitude faster than those  
38 in the bulk.<sup>1-7</sup> Although the underlying mechanism remains unclear, three main factors are thought  
39 to contribute—increased concentrations due to solvent evaporation, surface acidity (i.e. charge),  
40 and interfacial adsorption.<sup>8</sup> Many studies reporting enhanced rates of reaction have used an  
41 electrospray source to generate an aerosol plume.<sup>1-5</sup> Electrospray sources produce highly charged  
42 and rapidly evaporating droplets, which could lead to increasing reactant concentrations,  
43 significant pH variability compared to the bulk (due to solvent oxidation by the charges in the  
44 droplets), and complex ion-ion and ion-solvent interactions. Further, the droplet plume exhibits a  
45 high surface area relative to the bulk volume, thus enhancing the role of interfacial adsorption in  
46 perturbing chemical kinetics.<sup>8</sup> An increase in the surface to volume ratio of the droplets has been  
47 found to increase the reaction rate, suggesting the droplet surface could play a major role in the  
48 observed rate acceleration.<sup>7</sup> Most measurements studying rate enhancements in microdroplets use  
49 a polydisperse droplet source, which limits the control of both size distribution and time evolution  
50 of the reactant concentration.<sup>1-6</sup> Microfluidic devices capable of generating a monodisperse droplet  
51 distribution have also been used to study rate enhancements in microdroplet emulsions.<sup>7</sup> However,  
52 it remains unclear if the rate enhancing properties attributed to the oil-water interface of  
53 microfluidic devices are general to the air-water interface.

54 Another means of ensuring a monodisperse size is by limiting a study to a single droplet.  
55 The contactless confinement of single, micron-sized droplets has been established as a powerful  
56 method for probing the physical and chemical properties of liquids and heterogeneous interfaces.<sup>9</sup>

57 For example, aerosol optical tweezers (AOT) have been used to measure the surface tension,  
58 viscosity and hygroscopicity of a wide variety of aqueous samples, while electrodynamic balance  
59 (EDB) methods have allowed rapid mass transport and transformation processes to be  
60 interrogated.<sup>9</sup> AOT provide powerful, real-time characterization of droplets via the morphology  
61 dependent resonances that appear in the Raman spectrum of the droplet induced by the trapping  
62 laser. Also, a holographic optical trap (HOT) can manipulate arrays of droplets, and bring selected  
63 droplets into contact when desired. All droplets confined in a HOT can be fully characterized using  
64 cavity enhanced Raman spectroscopy to determine their size to nanometer accuracy before they  
65 are mixed together.<sup>10</sup> EDB's are extremely versatile techniques and offer advantages over AOT  
66 methods due to the facile introduction of single droplets into the confinement region and the ability  
67 to trap particles that strongly absorb laser light. EDB's can trap a larger range of droplet sizes than  
68 AOT (from 100s of nanometers<sup>11</sup> to 100  $\mu\text{m}$  diameter for EDB's<sup>9</sup> compared with  $<10 \mu\text{m}$  for  
69 AOT<sup>10</sup>). A wide range of electrode configurations have been developed (e.g. double ring,  
70 cylindrical, quadrupole) to facilitate a broad range of measurements, including the study of Mie  
71 scattering,<sup>12</sup> hygroscopicity and phase transitions,<sup>13,14</sup> heterogeneous chemistry,<sup>15,16</sup> ice  
72 nucleation,<sup>17-19</sup> and mass transport from droplets.<sup>20,21</sup> In these measurements, compositional  
73 changes in confined particles are typically the result of interfacial processes, such as mass transport  
74 (evaporation and/or condensation of semi-volatile and volatile material) or chemical changes due  
75 to reactive gas uptake. This makes bulk initiated chemistry difficult to study in conventional EDB  
76 configurations because it is hard to initiate a reaction cleanly at a well-defined time in a single  
77 droplet with no external reactant source.

78         The optical probes, such as Raman spectroscopy, that are typically used to characterize  
79 droplets in an EDB or AOT are limited to functional group information and cannot provide

80 information about the exact chemical composition of the droplet as it undergoes reactive  
81 transformations.<sup>9</sup> As evident from previous rate enhancement measurements,<sup>1-6</sup> mass spectrometry  
82 of droplets can provide quantitative chemical information, but studies characterizing single  
83 droplets with mass spectrometry are limited. Previously, free-falling droplets have been ionized  
84 directly by impaction on a highly charged needle, forming a spray that is directed toward a mass  
85 spectrometer.<sup>22</sup> Several studies have performed mass spectrometry on single, levitated droplets in  
86 an acoustic trap (which uses ultrasonic waves to confine particles) coupled to a laser desorption<sup>23,24</sup>  
87 or a direct analysis in real time (DART) ionization source.<sup>25</sup> However, because of the strong  
88 electric fields in EDB's and the small size of the trapped droplet, non-destructive mass  
89 spectrometry is difficult (i.e. particles need to be removed from the trap and ionized completely).  
90 Previous work has shown droplets can be ejected from a double ring electrode, deposited onto a  
91 matrix and ionized using matrix assisted laser desorption ionization.<sup>26</sup> However, the delay between  
92 deposition and detection is not ideal for real time reaction monitoring, and direct ionization of  
93 droplets as they exit the EDB is preferred. Very recently, work has quantified evaporation from  
94 microdroplets by ejecting single droplets from a double ring electrode, vaporizing them on a heated  
95 platform and ionizing the components using a corona discharge.<sup>27</sup>

96 In order to further explore chemical transformations in micron-sized compartments, we  
97 present here a new EDB electrode arrangement—the branched quadrupole trap (BQT)—that is  
98 capable of merging confined droplets. Merged droplets have previously been trapped using a  
99 tandem electrodynamic trap and observed spectroscopically.<sup>28</sup> The BQT allows for rapid changes  
100 in composition via droplet coalescence (enabling the study of bulk initiated processes) and allows  
101 for the ejection of single droplets into an ionization source for mass spectral analysis (enabling  
102 chemical characterization of droplets). By coupling droplet confinement techniques with high

103 resolution mass spectrometry, it is possible to measure condensed phase chemical kinetics in  
104 micro-compartments under well-defined conditions. Due to the droplet size range over which EDB  
105 methods operate (1 – 10's  $\mu\text{m}$ ) and their ability to control droplet composition by changing  
106 environmental conditions, they represent a unique way to study chemical reactions in a potentially  
107 interesting droplet size regime. In this work, we characterize the mixing times of merged droplets  
108 and demonstrate the application of the technique to probing chemical processes in droplets using  
109 both fluorescence spectroscopy and single droplet paper spray (PS) mass spectrometry.

## 110 **II. Experimental Section**

### 111 **a. Branched Quadrupole Trap Design**

112 A linear quadrupole EDB allows arrays of droplets to be confined along the axis of four  
113 rods, as has been discussed previously.<sup>11,29</sup> In order to facilitate merging of different droplet  
114 populations, the branched quadrupole trap (BQT) design has been developed (shown in Figure 1).  
115 Aqueous droplets are generated using a piezoelectric dispenser with a 50  $\mu\text{m}$  orifice (Microfab,  
116 Inc.) and are introduced into the top of the BQT along the linear axis. During actuation of the  
117 dispenser, high voltage (typically <1 kV) is applied to an induction electrode to induce a net charge  
118 on the droplet allowing it to become confined within the electric field of the BQT. Droplets  
119 generally have a net charge on the order of  $10^{-13}$  C ( $\sim 10^6$  elementary charges),<sup>30</sup> which leads to  
120 surface charge densities that are  $\sim 100$  times smaller than those found in electrospray droplets.<sup>31</sup>  
121 The BQT consists of four stainless steel trapping electrodes arranged in a quadrupole  
122 configuration. An alternating voltage ( $V_{ac}$ ) with an amplitude of 300-500 V and frequency of 200-  
123 400 Hz is applied to the trapping electrodes to confine the charged droplets axially along the rods.

124 A set of branching electrodes that extend off the linear trap at a  $60^\circ$  angle allow two  
125 separate droplet dispensers with to be used concurrently or simultaneously. By using two different  
126 solutions in each of the dispensers, chemistry can be initiated when droplets from each of the  
127 dispensers collide. Droplets dispensed from both the vertical dispenser and branch dispenser travel  
128  $\sim 12$  cm before they enter the common, lower portion of the trap. Droplets are held in the lower  
129 trap using a set of balancing electrodes that consist of stainless steel blades extending  
130 symmetrically between the rods toward the center of the quadrupole trap. By applying a static  
131 voltage (up to  $\pm 500$  V) to these electrodes, the gravitational force acting on the droplet can be  
132 overcome, leading to contactless levitation of the droplet.

133 Once confined within the trap, droplets are illuminated with a 532-nm laser (Changchun  
134 New Industries Optoelectronic Tech.) introduced axially. Scattered light from the laser is collected  
135 (using an optical scheme that has been previously reported)<sup>32</sup> and imaged in the far field with a  
136 CMOS camera (Thorlabs, Inc.) using a 532-nm line pass filter. The far field image serves two  
137 purposes: droplet positioning and sizing. A feedback loop controlling the voltage applied to the  
138 balancing electrodes is used to keep the droplet centered in the far field image and stationary in  
139 the trap. For example, as a droplet evaporates and loses mass, the magnitude of the voltage applied  
140 to hold the droplet decreases to keep the droplet fixed in space. Additionally, the far field image  
141 contains interference fringes from Mie scattering with distinct maxima and minima. The angular  
142 spacing of these fringes, the wavelength of scattered light (532 nm) and the refractive index of the  
143 droplet (1.36 for the  $\sim 3$  M LiCl droplets)<sup>33</sup> are used with the geometrical optics approximation to  
144 determine the radius of the droplet.<sup>34</sup> An additional 355-nm laser (JDS Uniphase) is introduced co-  
145 axially with the 532 nm laser and is used to excite fluorescence in the confined droplet.

146           The BQT is housed within an environmentally controlled chamber and most experiments  
147 were performed in a high relative humidity (RH ~90 %) atmosphere generated by passing 200-500  
148 sccm of nitrogen gas through a water bubbler. The RH of the gas is measured with two separate  
149 RH sensors (Honeywell International, Inc.) located at the inlet and outlet of the chamber. The  
150 nitrogen flow exerts a downward force on the trapped droplets and facilitates droplet ejection into  
151 the mass spectrometer when the DC trapping voltage is removed.

#### 152 **b. Merging Droplets in the BQT:**

153           In a typical merging experiment, a single droplet is dispensed from the side arm dispenser  
154 and held in the lower trap. A second droplet from the vertical dispenser is generated and merges  
155 with the confined droplet. The voltages applied to the induction electrodes are set to produce  
156 droplets of opposite polarity (droplets with the same charge polarity will not merge). The initial  
157 droplet (from the side arm dispenser) has a larger net charge than that from the vertical dispenser.  
158 When droplets merge, there is a decrease in the overall charge and an increase in the mass of the  
159 droplet, which both cause the merged droplet to fall lower in the trap. The initial position of the  
160 droplet is restored by increasing the voltage applied to the balancing electrodes using the voltage  
161 feedback loop. Droplet size is determined from the fringe separation from Mie scattering in the far  
162 field image both before and after merging the event. The change in radius with the merging event  
163 is used to infer the size of the merged droplet. As shown in Figure 2, the radii of the triggered and  
164 merged droplets are very repeatable ( $\pm 200$  nm, 0.7 % relative standard deviation). The size of the  
165 held droplet is controlled by changing the water activity of the initial solution with a soluble salt  
166 (~0.4-6 M LiCl) and allowing the droplet to equilibrate with the trap conditions. The size of the  
167 merging droplet is controlled by changing the shape (i.e., magnitude and duration) of the square  
168 wave electrical pulse used to generate the droplet with the piezoelectric microdispenser.<sup>35</sup> As the

169 merging droplet diameter increases, its terminal velocity changes from 0.07 to 0.15 m/s for 39 and  
170 55  $\mu\text{m}$  diameter droplets, respectively. Compared to previously reported droplet merging  
171 approaches in an EDB,<sup>28</sup> the BQT approach does not separate droplet coalescence from  
172 spectroscopic study. Thus, fast reactions (such as mixing dynamics in droplets) can easily be  
173 studied using the BQT.

174 We have applied two different methods to study the merging process and the evolving  
175 chemical composition of droplets. Fluorescence emitted by the droplet is collected and focused  
176 onto a photomultiplier tube (PMT, Hamamatsu Photonics) using a plano-convex lens ( $f/30$  mm).  
177 The fluorescence emitted by the droplet is used to quantify mixing times and reaction kinetics. A  
178 paper spray (PS) ionization source is used for single droplet mass spectrometry measurements to  
179 detect the products of a reaction.

### 180 **c. Mixing Times from Droplet Fluorescence:**

181 The mixing time in a merged droplet is measured to determine the fastest reactions that can  
182 be studied using the BQT. This time is measured by quantifying the acid-induced quenching of  
183 Rhodamine-B (RhB), a fluorescent dye. Fluorescence from a droplet containing 500  $\mu\text{M}$  RhB and  
184 LiCl is excited using the 532 nm laser and detected with the PMT using a 550 nm long pass filter  
185 to remove any elastically scattered light. Fluorescence from the RhB droplet is quenched by  
186 merging it with a sulfuric acid droplet (2-20% v/v). The decay of fluorescence intensity upon  
187 droplet coalescence is measured with the PMT (data acquisition rate = 500 kHz). Mixing is studied  
188 by: 1) changing the size of the trapped droplet and keeping the size of the merging droplet constant;  
189 2) keeping the size of the trapped droplet constant and changing the size of the merging droplet;  
190 and 3) changing the concentration of sulfuric acid in the merging droplet.



#### 191 **d. Reaction Kinetics from Droplet Fluorescence:**

192 Fluorescence is used to measure chemical kinetics in a single droplet which can be directly  
193 compared to those in the bulk solution. The chemical reaction between ortho-phthalaldehyde  
194 (OPA) and alanine in the presence of dithiothreitol (DTT) yields an isoindole product that  
195 fluoresces at ~400-500 nm (Scheme 1).<sup>36,37</sup> Solutions of OPA and alanine are prepared in a 3 M  
196 LiCl solution that is buffered with a 50 mM borate buffer (pH = 9). Alanine solutions have  
197 concentrations of 5.3, 10.3, 15.3, 20.8 and 33.3 mM. OPA and DTT are mixed together (to form a  
198 stable adduct)<sup>37</sup> and have concentrations of 5.3 mM and 7.8 mM, respectively. Fluorescence from  
199 merged alanine and OPA droplets is excited by the 355 nm laser and measured with the PMT using  
200 a 450±20 nm bandpass filter to remove elastically scattered laser light. At least 10 trials are used  
201 for each reaction condition in the droplets. Reaction kinetics measured in droplets are compared  
202 to those measured in the bulk as described in the Supporting Information.

#### 203 **e. Single Droplet Paper Spray Mass Spectrometry:**

204 By coupling a paper spray (PS) ionization source to the exit of the BQT, we have developed  
205 a new approach to determine how the chemical composition of a single droplet changes over the  
206 course of a reaction. A schematic of the experimental setup is shown in Figure 3a. The details of  
207 PS mass spectrometry and its applications have been previously described.<sup>38,39</sup> Here, a PS  
208 ionization source is generated by cutting a small triangle (~6 mm base, ~10 mm height) from  
209 chromatography paper (Whatman 3MM), passing a solvent through it, and applying a 4-5 kV  
210 potential. The tip of the PS is placed ~2.5 cm from the inlet of the mass spectrometer (Q-Exactive  
211 Orbitrap, Thermo Fisher Scientific, Inc.). The large electric field at the tip of the paper causes a  
212 spray to form that is directed toward the mass spectrometer. A 0.8-1.0 mL/hour flow of 1% formic  
213 acid solution in methanol through the filter paper maintains continuous operation of the PS source.

214 The mass spectrometer was operated with a resolution of 17,500 and a maximum ion injection  
215 time of 50 ms.

216 A 2-cm long piece of 1/4" stainless steel tubing is affixed to the exit of the BQT coaxial with  
217 the trap. The BQT is positioned such that the exit of this tubing is ~1 cm above the tip of the PS  
218 source. After merging, droplets are held in the trap for a fixed period of time. Following a delay,  
219 the voltage applied to the balancing electrodes is removed and the droplet falls from the trap  
220 (typically aided by the flow of humidified nitrogen), impinging on the tip of the PS source. The  
221 flow of solvent dilutes the droplets and pushes the components in the droplet toward the tip of the  
222 filter paper where they are ionized and sprayed into the mass spectrometer. Compared to  
223 electrospray techniques with droplets,<sup>40</sup> the PS source slows down the ionization event and ensures  
224 the entire droplet is sampled. Figure 3b shows a mass spectrum that is collected from a single, 50  
225  $\mu\text{m}$  diameter droplet of 0.2% citric acid (~0.6 ng of citric acid total). Due to its low vapor pressure  
226 and previous use in our lab,<sup>41</sup> citric acid is used to benchmark the sensitivity and reproducibility  
227 of the single droplet PS mass spectrometry technique. The mass spectrometer is operated in  
228 negative mode and the only peak observed is from deprotonated citric acid ( $[\text{M-H}]^-$ ) at  $m/z$  191.  
229 Figure 3c shows the time profile of the peak at  $m/z$  191. Each individual spike arises from the  
230 impact of one droplet on the PS source. The average peak area of these droplets has a relative  
231 standard deviation of ~15% (likely due to variation in where the droplet impacts the PS source).  
232 The precision of this method could be improved with the use of an internal standard in the droplet.

233 The products of the reaction between OPA and alanine in the absence of LiCl are studied  
234 using single droplet PS mass spectrometry. Because the large amount of LiCl that is used in the  
235 fluorescence experiments significantly diminishes the ionization efficiency of the organic species  
236 by the PS source, LiCl is not added for the single droplet mass spectrometry experiments. Solutions

237 of 10.7 mM OPA with 21.4 mM DTT and 30.0 mM alanine are prepared in a 50 mM borate buffer  
238 (pH ~ 9). The mass spectrometer is operated in positive ion mode to study both the components of  
239 pure, unreacted OPA and alanine droplets as well as merged, reacted droplets.

### 240 **III. Results and Discussion:**

241 In order to facilitate an understanding of the observed reaction kinetics, we first describe  
242 the mixing times that are observed in merged droplets and the experimental parameters that control  
243 them. Then, both kinetic and product analyses of the reaction between OPA and alanine in droplets  
244 are presented. Reaction kinetics measured with fluorescence imaging are reported in Section III.b.  
245 The OPA/alanine reaction products that were observed with single droplet PS mass spectrometry  
246 are presented in Section III.c.

#### 247 **a. Mixing Times in Merged Droplets:**

248 The fastest reaction kinetics that can be measured in a well-mixed droplet following  
249 coalescence is dependent on the timescale for mixing in the merged droplets. Here, the time it  
250 takes for a merged droplet to mix completely is measured by quantifying the quenching rate of a  
251 fluorescent dye. RhB fluorescence is quenched by a change in pH of solution; at low pH  
252 fluorescence is quenched almost entirely (Figure S-1, Supporting Information). Figure 4a shows  
253 examples of how the fluorescence from differently sized RhB droplets (500  $\mu$ M) is quenched when  
254 they merge with 20% (v/v) sulfuric acid droplets of a constant diameter ( $38 \pm 3$   $\mu$ m). The initial rise  
255 in fluorescence intensity is due to the increase in the cross sectional area of the droplet illuminated  
256 by the laser. As the coalesced droplet relaxes from initially dumbbell-shaped to spherical, its cross  
257 sectional area changes, causing the observed fluorescence intensity to oscillate. A similar effect is  
258 observed (and has been reported previously<sup>42</sup>) in elastically scattered light (Figure S-2, Supporting

259 Information). The angular frequency and damping of this oscillation is related to the surface  
 260 tension and viscosity of the merged droplet, respectively.<sup>42</sup> Droplets typically relax to a spherical  
 261 shape after  $\sim 200 \mu\text{s}$ . The fluorescence transients are fit to the following piecewise exponential  
 262 decay function to extract mixing times:

$$263 \quad I = \begin{cases} a + b, & t < c \\ a \cdot e^{-(t-c)/d} + b, & t \geq c \end{cases}, \quad (1)$$

264 where  $a$  is the quenched fluorescence intensity,  $b$  is the fluorescence intensity post-quenching,  $c$   
 265 is the time delay between data collection and droplet merging, and  $d$  is the mixing time. The red  
 266 lines shown in Figure 4a are the fits of Eq. 1 to the fluorescence transients. Because the lifetimes  
 267 of surface oscillations are typically shorter than the observed mixing times and their magnitude is  
 268 less than the change due to quenching, surface oscillations are not explicitly considered in Eq. 1.

269 To better understand the observed mixing times, they are compared to the timescales for  
 270 molecular diffusion, viscous diffusion, and bulk convection. The characteristic time for molecular  
 271 diffusion ( $\tau_{Diff}$ ) is:

$$272 \quad \tau_{Diff} \sim \frac{L_{ch}^2}{D}. \quad (2)$$

273 This is the time needed for a molecule to diffuse one characteristic length ( $L_{ch}$ ) in a fluid with mass  
 274 diffusivity  $D$ . For RhB in water,  $D$  is  $4.2 \pm 0.3 \times 10^{-10} \text{ m}^2 \text{ s}^{-1}$ .<sup>43</sup>  $L_{ch}$  for the merged droplet is  
 275 calculated from the held ( $D_{held}$ ) and merging ( $D_{merge}$ ) droplet diameters as follows:<sup>44</sup>

$$276 \quad L_{ch} = \frac{2D_{held}D_{merge}}{D_{held} + D_{merge}}. \quad (3)$$

277 For the droplet conditions here, molecular diffusion time is typically  $\sim 1-10 \text{ s}$ .

278 The viscous diffusion timescale ( $\tau_{visc}$ )—which represents the time required for momentum  
279 to diffuse one characteristic length scale in a fluid with kinematic viscosity  $\nu$ —is:

$$280 \quad \tau_{visc} \sim \frac{L_{ch}^2}{\nu}. \quad (4)$$

281 For a  $\sim 3$  M LiCl solution,  $\nu$  is  $1.4 \times 10^{-6} \text{ m}^2 \text{ s}^{-1}$ .<sup>45</sup> For the droplet conditions here, viscous diffusion  
282 is typically 1-10 ms.

283 Finally, the bulk convection timescale ( $\tau_{conv}$ ) is the time required for material to traverse  
284 one characteristic length at a rate equal to the relative droplet velocity ( $U_{rel}$ ):

$$285 \quad \tau_{conv} \sim \frac{L_{ch}}{U_{rel}}. \quad (5)$$

286 The relative velocity of the collision is calculated from the terminal velocity of the merging droplet  
287 (0.07-0.15 m/s). As the merging droplet approaches the balancing electrode, its velocity increases  
288 slightly due to Coulombic attraction. However, based on the voltage applied to the balancing  
289 electrode, this acceleration is measured to be small (Supporting Information, Figure S-3). For  
290 droplets here, the bulk convection time is typically  $\sim 200$ -600  $\mu\text{s}$ . Carroll and Hidrovo previously  
291 demonstrated that as the inertia of the collision event increases, the observed mixing times is  
292 shortened toward the bulk convection timescale.<sup>44</sup>

293 Figure 4b shows the measured mixing times when the size of the held droplet is changed  
294 and the diameter of the merging droplet is held constant ( $D_{merge} = 38 \pm 3 \mu\text{m}$ ). As the size of the  
295 held droplet decreases, the observed mixing time decreases toward the convection mixing time. A  
296 log-log plot of initial droplet diameter vs. mixing time has a slope of  $3.2 \pm 0.2$  (Figure S-4,  
297 Supporting Information), implying that the mixing rate in this experiment scales with the volume  
298 of the held droplet.

299 Figure 4c shows the mixing times when the size of the held droplet is constant ( $D_{held} =$   
300  $56 \pm 2 \mu\text{m}$ ) and the diameter of the merging droplet is changed. As the diameter of the merging  
301 droplet increases, the diameter of the merged droplet increases (which causes the viscous diffusion  
302 time to increase), and the terminal velocity of the merging droplet increases (which causes the bulk  
303 convection time to decrease). The experimental data show that mixing times decrease with  
304 increasing merging diameter. This is likely due to the increasing energy and inertia of the  
305 collision.<sup>44</sup> If the inertia of the collision were to continue to increase, the mixing time is predicted  
306 to follow the bulk convection time.<sup>44</sup> Finally, when the concentration of sulfuric acid is changed  
307 (and the held/merging droplet diameters are kept constant), the mixing times do not change (Figure  
308 S-5, Supporting Information). This suggests that the observed mixing times are controlled by the  
309 size of droplets and velocity of collisions, and are not due to the concentration of reagents in the  
310 in the droplets.

311 The observed mixing times reported here (reliably down to  $\sim 400 \mu\text{s}$ ) are very similar to  
312 those reported in free-droplet collision experiments (i.e. colliding droplets are not confined within  
313 an electrodynamic balance).<sup>46</sup> They are also similar to those observed in conventional stopped flow  
314 kinetics measurements ( $\sim 2 \text{ ms}$ ),<sup>47</sup> but slower than those achieved in miniaturized continuous flow  
315 methods such as theta capillary electrospray (mixing time  $\sim 1 \mu\text{s}$ )<sup>48</sup> and microfluidic channels  
316 (mixing time  $\sim 15 \mu\text{s}$ ).<sup>47</sup> Work by Lee *et al.* colliding a plume of high speed (80 m/s) 13- $\mu\text{m}$   
317 droplets report mixing times of a couple of microseconds.<sup>6</sup> The mixing times in the BQT allow for  
318 the study of reactions with a bimolecular rate constant of up to  $\sim 10^4$ - $10^5 \text{ M}^{-1} \text{ s}^{-1}$ . As shown, faster  
319 mixing times could be achieved by either using smaller droplets or increasing the velocity of the  
320 collision. The latter could be accomplished either electrostatically (e.g. apply a higher potential to  
321 the balancing electrodes, Figure S-3) or with a faster flow of gas through the trap.

## 322 **b. Chemical Reactions in Merged Droplets**

323           The reaction between OPA and alanine in the presence of DTT (Scheme 1) is studied in  
324 droplets with the BQT and bulk solution using fluorescence spectroscopy. LiCl is added to the  
325 solutions to decrease the water activity such that evaporation from the droplet is minimized and  
326 the conditions in the droplet can be reproduced in the bulk. Because the water activity of a 3.0 M  
327 LiCl solution is 0.87,<sup>49</sup> experiments are performed with a RH close to 87%, and the size of the  
328 droplet does not change considerably over time of the experiment (Figure S-6, Supporting  
329 information). In bulk measurements, the volumes of the reactant solutions are mixed in a 1:1 ratio,  
330 and the initial reactant concentrations are half the value of the prepared solutions. In droplets, the  
331 initial reactant concentrations are determined using the size of the merging droplets ( $24.3 \pm 0.2 \mu\text{m}$   
332 and  $23.0 \pm 0.6 \mu\text{m}$  radius for alanine and OPA, respectively). The merged droplet has a radius of  
333  $29.9 \pm 0.4 \mu\text{m}$ . While keeping the initial OPA concentration constant ( $\sim 2.6 \text{ mM}$ ), the rate of  
334 fluorescence appearance is measured at various alanine concentrations ( $\sim 2.6, 5.2, 7.7, 10.4$  and  
335  $16.7 \text{ mM}$ ). Figure 5 shows an example of the bulk and droplet fluorescence data that are collected  
336 with  $\sim 2.6$  and  $\sim 7.7 \text{ mM}$  initial OPA and alanine concentrations, respectively. Fluorescent intensity  
337 in the droplet appears at a slightly faster rate than in the bulk solution. To quantify the reaction  
338 rate constants in the merged droplet and bulk, the OPA and alanine reaction is simulated and fit to  
339 experimental data.

340           When the alanine concentration exceeds the OPA concentration, the final fluorescence  
341 intensity does not change with increasing amounts of alanine. At these conditions, it is assumed  
342 that the final concentration of the fluorescent product is equal to that of the initial OPA  
343 concentration. Using this scaling, the measured fluorescence intensity is converted to  
344 concentration of fluorescent product. The reaction between OPA and alanine has previously been

345 shown to follow bimolecular kinetics.<sup>36</sup> Thus, to quantify the rate of reaction in bulk and droplets,  
346 an ordinary differential equations solver is used to simulate a bimolecular reaction with the initial  
347 reactant concentrations set to experimental values. The bimolecular rate constant in the simulation  
348 is varied to best match the simulated and experimental product concentrations. The same kinetic  
349 analysis is used for both bulk and droplet experiments. The solid lines in Figure 5 represent the  
350 simulated product concentrations with the optimized rate constant. The average bimolecular  
351 reaction rate constants in the bulk and droplet are  $67\pm 6$  and  $84\pm 10$   $\text{M}^{-1} \text{s}^{-1}$ , respectively.  
352 Uncertainty corresponds to the standard deviation of the rate constants extracted at each reaction  
353 condition. The simulated fits and individual rate constants extracted at each reactant condition are  
354 tabulated in the Supporting Information (Figure S-7 and Table S-1). The bimolecular rate constant  
355 for the reaction of alanine with OPA in the presence of DTT has previously been measured to be  
356  $60\pm 4$   $\text{M}^{-1} \text{s}^{-1}$ ,<sup>36</sup> which is in good agreement with the bulk rate constant reported here.

357         The average rate constant in the 30  $\mu\text{m}$  radius droplet is roughly 25% larger than the rate  
358 constant in the bulk. When the polarity of the charge on the droplet is reversed (i.e. the merged  
359 droplet has a net positive charge instead of net negative charge) the kinetics of the reaction are  
360 unchanged (Figure S-8 in Supporting Information). This suggests that the small amount of charge  
361 on the droplet surface does not affect the overall rate of reaction. Because evaporation from the  
362 particle is minimized with the addition of LiCl, the small observed rate enhancement could  
363 originate from enhanced surface to volume ratio in the droplet compared to the bulk. Fallah-Araghi  
364 *et al.* previously measured the kinetics of a bimolecular reaction in aqueous droplets in an oil-  
365 water emulsion. They observed a maximum rate enhancement by factor of  $\sim 40$  that decreased with  
366 increasing droplet radius. The observed enhancement was attributed to the increasing surface to  
367 volume ratio at smaller droplet sizes. A weak adsorption of molecular species to the oil-water



368 interface was predicted to change the energetics of the reaction to favor product formation.  
369 However, a rate enhancement was only observed in emulsions that had a radius smaller than  $\sim 20$   
370  $\mu\text{m}$ .<sup>7</sup> The merged droplets in this study have a radius of  $29.4 \pm 0.4 \mu\text{m}$ , which could indicate that  
371 the droplets used here are still too large to observe a significant rate enhancement from interfacial  
372 effects.

### 373 **c. Single Droplet Mass Spectrometry**

374 The products of the reaction between OPA and alanine are studied using the PS ionization  
375 source. Figure 6a shows mass spectra from a single alanine droplet (black line) and OPA solution  
376 droplet (red line). Compared to the concurrently developed single droplet mass spectrometry  
377 method (which uses a corona discharge to ionize the vaporized droplet components),<sup>27</sup> the use of  
378 the PS ionization source leads to less fragmentation and easier identification of reaction products.  
379 The alanine spectrum has only one peak at  $m/z$  90, which represents the protonated molecular ion.  
380 The OPA spectrum has peaks at  $m/z$  135 and 157, which are from the protonated OPA molecule  
381 and the OPA/ $\text{Na}^+$  complex, respectively. The peak at  $m/z$  311 corresponds to the OPA and DTT  
382 adduct complexed with a  $\text{Na}^+$  ion. OPA reacts with thiol containing compounds to create a stable  
383 1,3-dihydroisobenzofuran compound that has been previously observed.<sup>37</sup> Because DTT has two  
384 reactive thiol groups, a single DTT molecule can react with two OPA molecules. The peak at  $m/z$   
385 445 corresponds to this reaction product complexed with a  $\text{Na}^+$  ion. Figure 6a also shows the mass  
386 spectrum of a single merged droplet after it has reacted for 6 s (blue line). Because alanine is in  
387 excess in the merged droplet, only the intensities of the peaks from OPA-containing species have  
388 decreased significantly (the alanine peak remains a dominant peak). The peaks present at  $m/z$  342  
389 and 476 correspond to the protonated isoindole reaction products.<sup>36,37</sup> The chemical structures for  
390 each of the ions are shown in the Supporting Information (Table S-2).

391 Figure 6b shows a selected ion chromatogram from the ejected merged droplets for each  
392 of the peaks of interest in the experiment ( $m/z$  90, 311, 342, 445, and 476). Each of the ions show  
393 a similar time response, and are only present when a droplet is ejected onto the PS source. A  $\sim 5$   
394 mM aqueous droplet with a radius of  $30\ \mu\text{m}$  (similar to the OPA conditions in this experiment) has  
395  $\sim 0.5$  pmol of material ( $< 1$  ng). As shown in Figure 6b, this results in single droplet pulses with a  
396 signal to noise (S/N) ratio  $> 100$ . Assuming a S/N ratio of  $\sim 10$  is necessary to quantify peak  
397 intensities, a single,  $\sim 5$ -mM droplet with a radius of  $\sim 15\ \mu\text{m}$  could easily be detected in the current  
398 configuration.

#### 399 **IV. Conclusion:**

400 A branched quadrupole trap has been designed and constructed to merge confined droplets.  
401 This trap allows for new measurements of homogeneous chemical reactions in droplets. Through  
402 the quenching of fluorescence of RhB droplets by sulfuric acid droplets, consistent mixing times  
403 as short as  $\sim 400\ \mu\text{s}$  are obtainable using droplets moving at relative velocities of  $\sim 0.1$  m/s. As  
404 predicted by Carroll and Hidrovo,<sup>44</sup> mixing experiments in the BQT show that faster mixing times  
405 are achievable by either decreasing the size of the merging droplets or increasing the speed of the  
406 collision. With these mixing times, chemical reactions with a bimolecular rate constant up to  $\sim 10^4$ -  
407  $10^5\ \text{M}^{-1}\ \text{s}^{-1}$  can be studied in the BQT in its current form.

408 The ability to measure homogeneous chemical reactions in the BQT has been demonstrated  
409 using both fluorescence spectroscopy and single droplet PS mass spectrometry. The reaction of  
410 OPA with alanine (in the presence of DTT) is found to occur slightly faster ( $\sim 25\%$ ) in a droplet  
411 with a radius of  $\sim 30\ \mu\text{m}$  than in bulk solution. Charge on the droplet and changes in the  
412 concentration of reactants due to evaporation do not play a significant role in any potential rate  
413 enhancement in the fluorescence experiments reported here. Thus, the small rate enhancement is

414 attributed to the larger surface to volume ratio of the droplet compared to the bulk. Single droplet  
415 PS mass spectra of reacted droplets following merging show the expected reaction products. Based  
416 on the observed signal levels, it is estimated that single droplets with a radius of  $\sim 15 \mu\text{m}$  with  $< 100$   
417 pg of analyte could be easily detected using PS mass spectrometry.

418 We have developed a new technique for the contactless manipulation and merging of  
419 micron-sized droplets to initiate chemistry. We demonstrate the applicability of fluorescence  
420 imaging for measuring reaction kinetics and demonstrate the use of mass spectrometry coupled  
421 with a single particle trap. Going forward, these developments will allow for rigorous probing of  
422 reaction kinetics in a variety of samples spanning a wide range of sizes and concentrations.

#### 423 **Acknowledgments:**

424 Early work on the design and construction of the BQT was supported by an Early Career  
425 Award (K.R.W. and J.F.D.) from the Condensed Phase and Interfacial Molecular Science Program,  
426 in the Chemical Sciences Geosciences and Biosciences Division of the Office of Basic Energy  
427 Sciences of the U.S. Department of Energy under Contract No. DE-AC02-05CH11231. The  
428 portion of this work on mixing timescales is supported by the Laboratory Directed Research and  
429 Development (LDRD) program at Lawrence Berkeley National Laboratory. M.I.J. is supported by  
430 a NSF Graduate Research Fellowship under DGE-1106400.

#### 431 **References:**

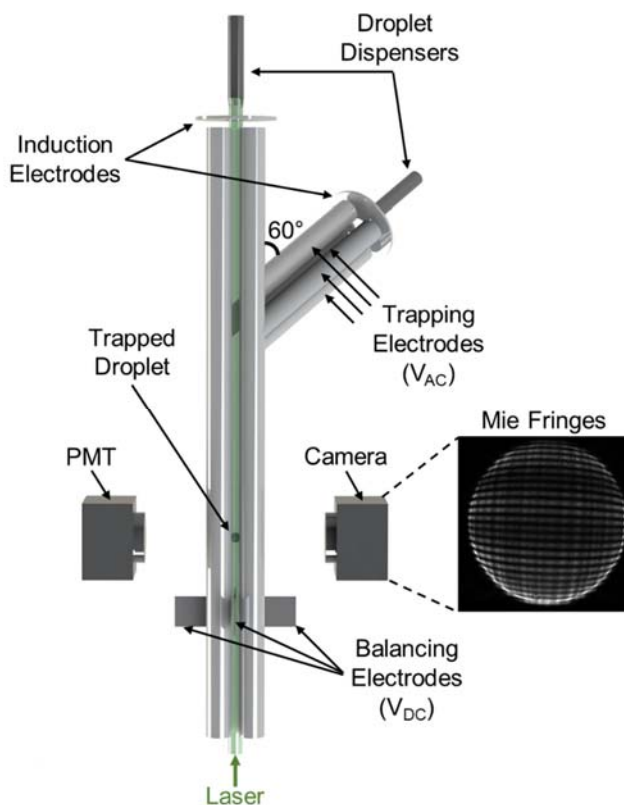
- 432 (1) Bain, R. M.; Pulliam, C. J.; Cooks, R. G. *Chem. Sci.* **2015**, *6* (1), 397–401.
- 433 (2) Girod, M.; Moyano, E.; Campbell, D. I.; Cooks, R. G. *Chem. Sci.* **2011**, *2* (3), 501.
- 434 (3) Banerjee, S.; Prakash, H.; Mazumdar, S. *J. Am. Soc. Mass Spectrom.* **2011**, *22* (10), 1707–  
435 1717.
- 436 (4) Müller, T.; Badu-Tawiah, A.; Cooks, R. G. *Angew. Chemie - Int. Ed.* **2012**, *51* (47),  
437 11832–11835.

- 438 (5) Banerjee, S.; Zare, R. N. *Angew. Chemie - Int. Ed.* **2015**, *54* (49), 14795–14799.
- 439 (6) Lee, J. K.; Kim, S.; Nam, H. G.; Zare, R. N. *Proc. Natl. Acad. Sci.* **2015**, *112* (13),  
440 201503689.
- 441 (7) Fallah-Araghi, A.; Meguellati, K.; Baret, J.-C.; Harrak, A. El; Mangeat, T.; Karplus, M.;  
442 Ladame, S.; Marques, C. M.; Griffiths, A. D. *Phys. Rev. Lett.* **2014**, *112* (2), 28301.
- 443 (8) Yan, X.; Bain, R. M.; Cooks, R. G. *Angew. Chemie - Int. Ed.* **2016**, *55* (42), 12960–12972.
- 444 (9) Krieger, U. K.; Marcolli, C.; Reid, J. P. *Chem. Soc. Rev.* **2012**, *41* (19), 6631–6662.
- 445 (10) Power, R. M.; Reid, J. P. *Reports Prog. Phys.* **2014**, *77* (7), 74601.
- 446 (11) Derkachov, G.; Kolwas, K.; Archer, J.; Wojciechowski, T.; Jakubczyk, D.; Kolwas, M.  
447 *Langmuir* **2015**, *31*, 7860–7868.
- 448 (12) Blau, H. H.; McCleese, D. J.; Watson, D. *Appl. Opt.* **1970**, *9* (11), 2522–2528.
- 449 (13) Tang, I. N.; Munkelwitz, H. R. *J. Geophys. Res.* **1994**, *99*, 18001–18808.
- 450 (14) Choi, M. Y.; Chan, C. K. *Environ. Sci. Technol.* **2002**, *36* (11), 2422–2428.
- 451 (15) Lee, A. K. Y.; Chan, C. K. *Atmos. Environ.* **2007**, *41* (22), 4611–4621.
- 452 (16) Pope, F. D.; Gallimore, P. J.; Fuller, S. J.; Cox, R. A.; Kalberer, M. *Environ. Sci. Technol.*  
453 **2010**, *44* (17), 6656–6660.
- 454 (17) Krieger, U. K.; Colberg, C. A.; Weers, U.; Koop, T. *Geophys. Res. Lett.* **2000**, *27* (14),  
455 2097–2100.
- 456 (18) Svensson, E. A.; Delval, C.; Von Hessberg, P.; Johnson, M. S.; Pettersson, J. B. C. *Atmos.*  
457 *Chem. Phys.* **2009**, *9* (13), 4295–4300.
- 458 (19) Hoffmann, N.; Kiselev, A.; Rzesanke, D.; Duft, D.; Leisner, T. *Atmos. Meas. Tech.* **2013**,  
459 *6* (9), 2373–2382.
- 460 (20) Davies, J. F.; Miles, R. E. H.; Haddrell, A. E.; Reid, J. P. *Proc. Natl. Acad. Sci. U. S. A.*  
461 **2013**, *110* (22), 8807–8812.
- 462 (21) Davies, J. F.; Haddrell, A. E.; Miles, R. E. H.; Bull, C. R.; Reid, J. P. *J. Phys. Chem. A*  
463 **2012**, *116* (45), 10987–10998.
- 464 (22) Tracey, P. J.; Vaughn, B. S.; Roberts, B. J.; Poad, B. L. J.; Trevitt, A. J. *Anal. Chem.*  
465 **2014**, *86*, 2895–2899.
- 466 (23) Westphall, M. S.; Jorabchi, K.; Smith, L. M. *Anal. Chem.* **2008**, *80* (15), 5847–5853.
- 467 (24) Warschat, C.; Stindt, A.; Panne, U.; Riedel, J. *Anal. Chem.* **2015**, *87* (16), 8323–8327.
- 468 (25) Crawford, E. A.; Esen, C.; Volmer, D. A. *Anal. Chem.* **2016**, *88* (17), 8396–8403.
- 469 (26) Bogan, M. J.; Agnes, G. R. *Anal. Chem.* **2002**, *74* (3), 489–496.
- 470 (27) Birdsall, A. W.; Krieger, U. K.; Keutsch, F. N. *Atmos. Meas. Tech. Discuss.* **2017**.

- 471 (28) Kohno, J. Y.; Higashiura, T.; Eguchi, T.; Miura, S.; Ogawa, M. *J. Phys. Chem. B* **2016**,  
472 *120* (31), 7696–7703.
- 473 (29) Hart, M. B.; Sivaprakasam, V.; Eversole, J. D.; Johnson, L. J.; Czege, J. *Appl. Opt.* **2015**,  
474 *54* (31), 174–181.
- 475 (30) Haddrell, A. E.; Davies, J. F.; Yabushita, A.; Reid, J. P. *J. Phys. Chem. A* **2012**, *116* (40),  
476 9941–9953.
- 477 (31) Wilm, M. *Mol. Cell. Proteomics* **2011**, *10* (7), M111.009407.
- 478 (32) Davies, J. F.; Haddrell, A. E.; Reid, J. P. *Aerosol Sci. Technol.* **2012**, *46* (6), 666–677.
- 479 (33) Gao, D.; Guo, Y.; Yu, X.; Wang, S.; Deng, T. *J. Chem. Eng. Data* **2015**, *60* (9), 2594–  
480 2599.
- 481 (34) Glantschnig, W. J.; Chen, S.-H. *Appl. Opt.* **1981**, *20* (14), 2499–2509.
- 482 (35) Vaughn, B.; Tracey, P.; Trevitt, A. *RSC Adv.* **2016**, *6*, 60215–60222.
- 483 (36) Trepman, E.; Chen, R. F. *Arch. Biochem. Biophys.* **1980**, *204* (2), 524–532.
- 484 (37) Zuman, P. *Chem. Rev.* **2004**, *104* (7), 3217–3238.
- 485 (38) Wang, H.; Liu, J.; Cooks, G. R.; Ouyang, Z. *Angew. Chemie - Int. Ed.* **2010**, *49* (5), 877–  
486 880.
- 487 (39) Lin, C. H.; Liao, W. C.; Chen, H. K.; Kuo, T. Y. *Bioanalysis* **2014**, *6* (2), 199–208.
- 488 (40) Dong, J.; Rezenom, Y. H.; Murray, K. K. *Rapid Commun. Mass Spectrom.* **2007**, *21*,  
489 3995–4000.
- 490 (41) Davies, J. F.; Wilson, K. R. *Chem. Sci.* **2015**, *6* (12), 7020–7027.
- 491 (42) Bzdek, B. R.; Power, R. M.; Simpson, S. H.; Reid, J. P.; Royall, C. P. *Chem. Sci.* **2016**, *7*,  
492 274–285.
- 493 (43) Gendron, P. O.; Avaltroni, F.; Wilkinson, K. J. *J. Fluoresc.* **2008**, *18* (6), 1093–1101.
- 494 (44) Carroll, B.; Hidrovo, C. *Heat Transf. Eng.* **2013**, *34* (2–3), 120–130.
- 495 (45) Ostroff, A. G.; Snowden, B. S.; Woessner, D. E. *J. Phys. Chem.* **1969**, *73*, 1968–1969.
- 496 (46) Takano, Y.; Kikkawa, S.; Suzuki, T.; Kohno, J. Y. *J. Phys. Chem. B* **2015**, *119* (23),  
497 7062–7067.
- 498 (47) Shastry, M. C. C.; Luck, S. D.; Roder, H. *Biophys. J.* **1998**, *74* (5), 2714–2721.
- 499 (48) Mortensen, D. N.; Williams, E. R. *Anal. Chem.* **2015**, *87* (2), 1281–1287.
- 500 (49) Robinson, R. A. *Trans. Faraday Soc.* **1945**, *41*, 756–758.

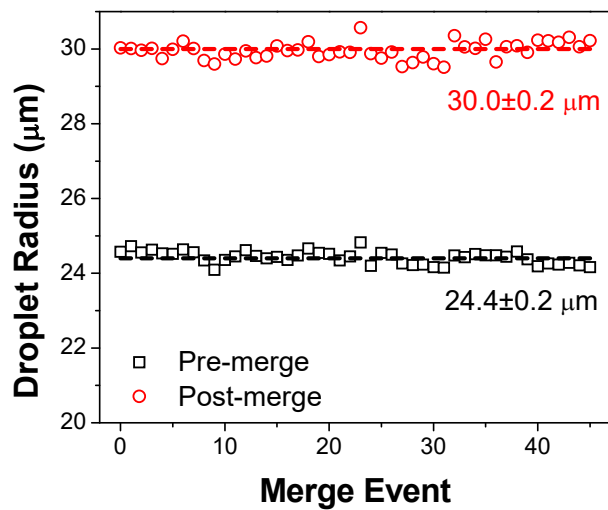
501

502



503  
 504 **Figure 1.** Schematic of the BQT. Different solutions necessary for a chemical reaction are  
 505 dispensed from the two droplet dispensers. Thus, when the droplets from each of the dispensers  
 506 coalesce, a chemical reaction in the merged, trapped droplet can be initiated. The chamber that  
 507 houses the BQT setup and the optics used to collect and collimate the light for the camera and  
 508 PMT are not shown. An example of the far field image of elastically scattered light used to  
 509 determine the size of the trapped droplet is shown.

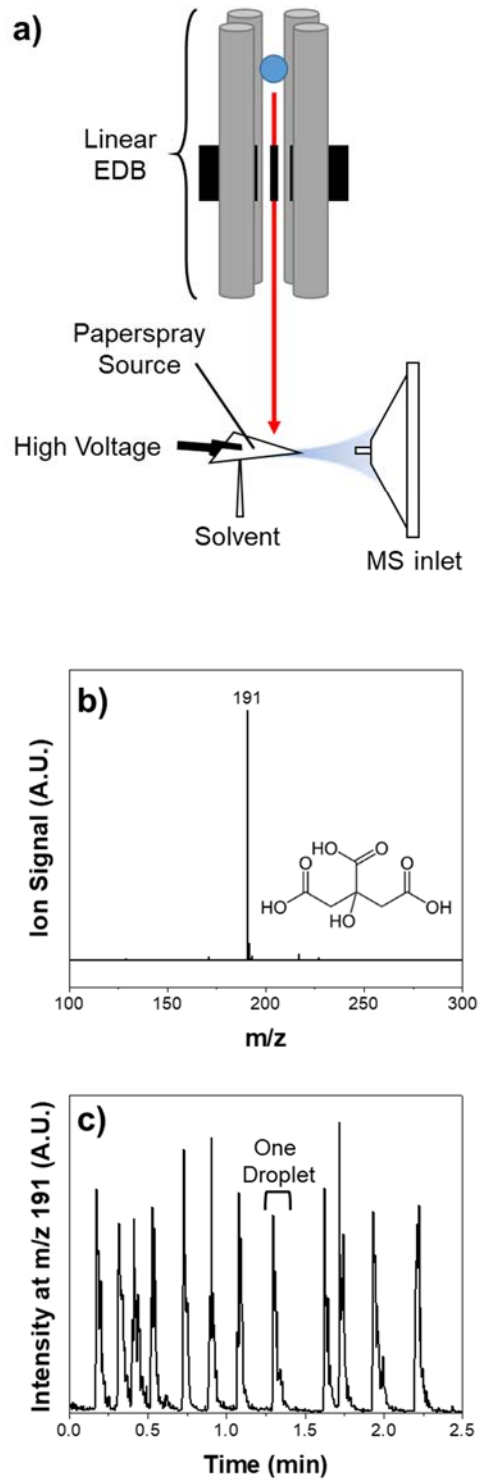
510



511  
512 **Figure 2.** Measured droplet radius before and after merging for 45 separate coalescence events  
513 (~2 hours of operation). Droplets contained ~3 M LiCl. The dashed lines show the average droplet  
514 radius.

515

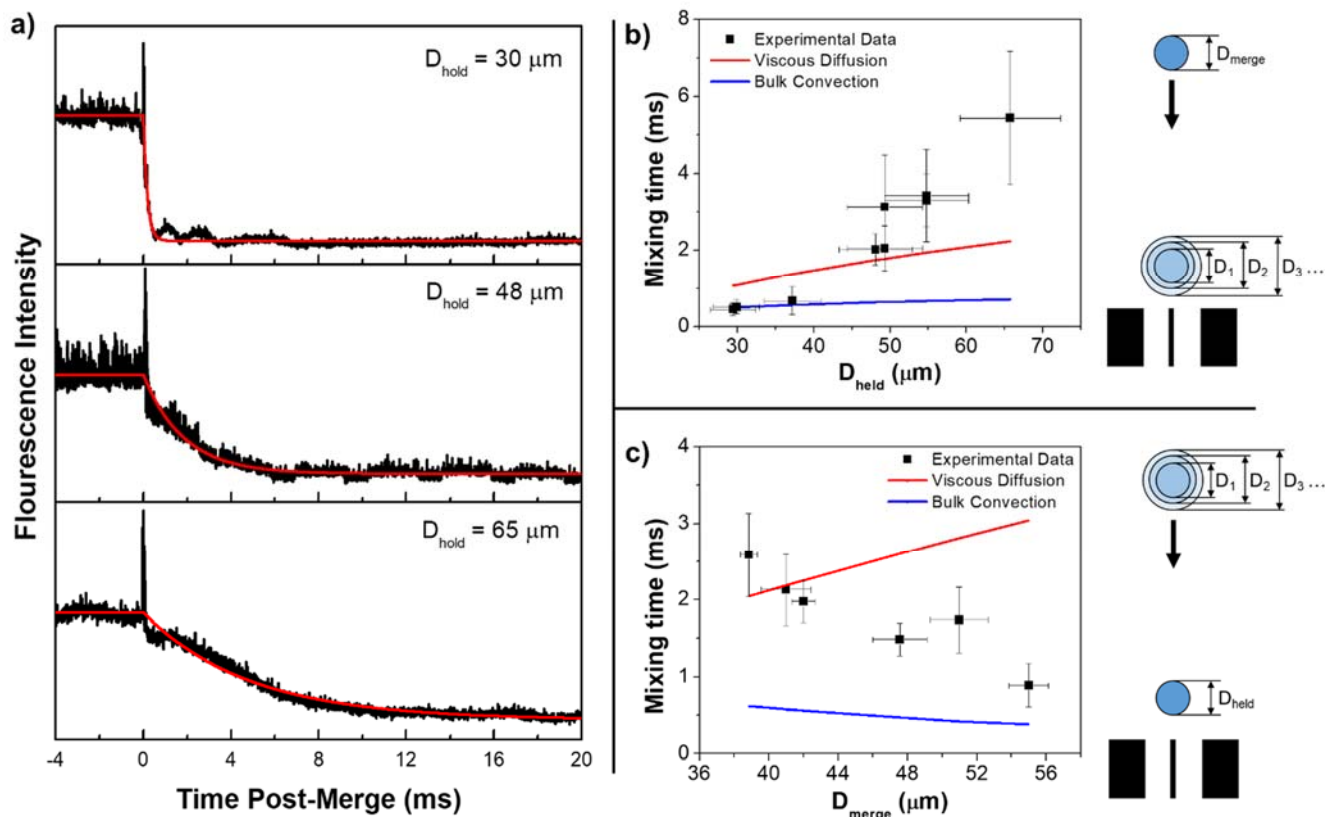
516



517

518 **Figure 3.** a) Schematic of the BQT/PS mass spectrometry interface. b) Mass spectrum from a  
 519 single 50- $\mu\text{m}$  diameter, 0.2% (w/v) citric acid droplet. c) Selected ion chromatogram of citric acid  
 520 droplets. Each spike in the chromatogram represents one 50- $\mu\text{m}$ , 0.2% citric acid droplet impacting  
 521 the PS source.

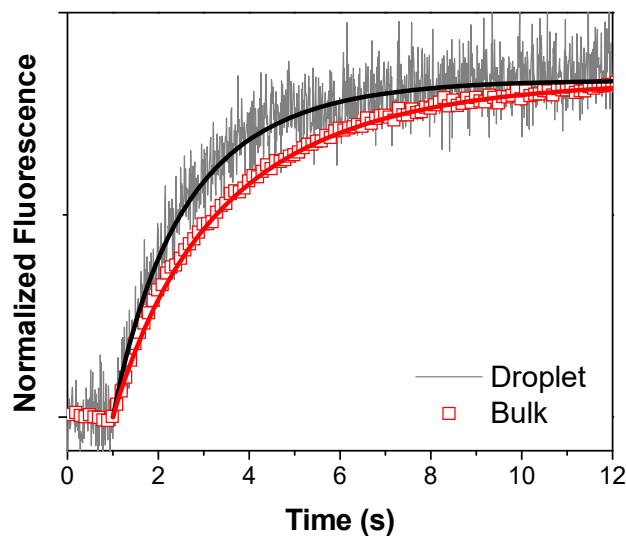




522

523 **Figure 4.** a) Fluorescent quenching of differently sized RhB droplets with the coalescence of a  
 524  $38 \pm 3 \mu\text{m}$ , 20% (v/v) sulfuric acid droplet. The fluorescence intensity measured with the PMT  
 525 (black line) is fit to Eq. 1 to extract a mixing time. The fit to the data is shown by the red line. The  
 526 data shown have mixing times of  $0.191 \pm 0.006$ ,  $1.82 \pm 0.03$  and  $4.93 \pm 0.06$  ms for the 20, 48, and 65  
 527  $\mu\text{m}$  RhB droplets, respectively. b) Mixing times for experiments where the merging droplet  
 528 diameter (sulfuric acid) is kept constant ( $38 \pm 3 \mu\text{m}$ ) and the held droplet diameter (RhB) is varied.  
 529 The viscous diffusion and bulk convection times are shown in red and blue, respectively. The  
 530 molecular diffusion times are too long to show on this scale. The experimental mixing times scale  
 531 with the volume of the held droplet. c) Mixing times for experiments where the merging droplet  
 532 diameter (sulfuric acid) is increased and the held droplet diameter (RhB) is kept constant ( $56 \pm 2$   
 533  $\mu\text{m}$ ). As the diameter of the merging droplet increases, the mixing time decreases.

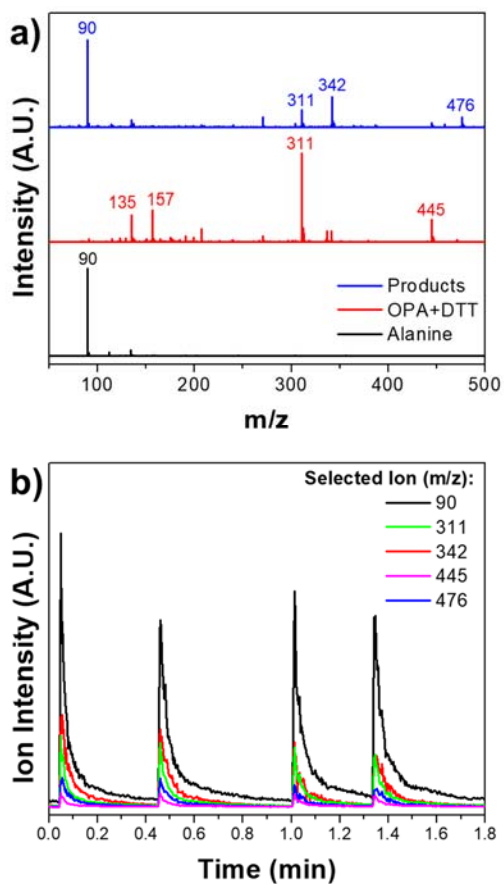
534



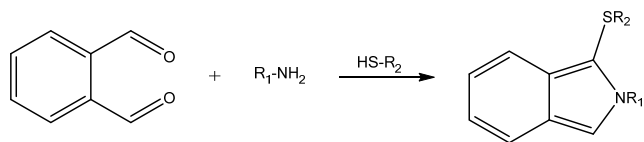
535

536 **Figure 5.** Fluorescence ( $450\pm 20$  nm) generated from the reaction of OPA with alanine in a droplet  
537 with a radius of  $29.9\pm 0.4$   $\mu\text{m}$  (gray line) and in bulk solution (red squares). In the droplet, the  
538 initial OPA concentration is  $2.4\pm 0.1$  mM and the initial alanine concentration is  $8.1\pm 0.4$  mM. In  
539 bulk solution, the initial concentration of OPA is 2.6 mM and the initial concentration of alanine  
540 is 7.7 mM. The solid black and red lines are the best-fit product concentrations from the  
541 bimolecular reaction simulation. The average bimolecular rate constant for the reaction of alanine  
542 with OPA is found to be  $84\pm 10$  and  $67\pm 6$   $\text{M}^{-1} \text{s}^{-1}$  in the droplet and bulk, respectively. The  
543 individual rate constants for the different reaction conditions are tabulated in Table S-1.

544



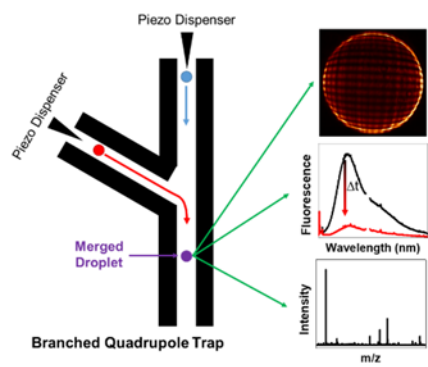
545  
 546 **Figure 6.** a) Mass spectra of single droplets from alanine solution (black line), OPA/DTT solution  
 547 (red line) and merged alanine/OPA droplets after 6 s of reaction (blue line). The new peaks in the  
 548 products spectrum (m/z 342 and 476) correspond to the expected fluorescent products. The  
 549 chemical structures of labeled peaks are given in the Supporting Information (Table S1). b)  
 550 Selected ion chromatograms showing the time response of each peak of interest in the merged  
 551 droplets. The signal to noise ratio for each of these peaks is >100.



552

553 **Scheme 1.** The reaction of ortho-phthalaldehyde (OPA) with a primary amine (alanine) in the  
554 presence of a thiol group (dithiothreitol, DTT) yields a fluorescent isoindole compound.

555



556

557 TOC Graphic